Article Journal of Asian Geography, 2025, Volume 4 (Issue 2), 46-62
https://doi.org/10.36777/jag2025.4.2.6

Satellite-Based Drought Monitoring Using Drought Indices in Salt Lake Meighan, Iran

S. Sajadi [1,*]

[1] Geoinformatic Unit, Geography Section, School of Humanities, Universiti Sains Malaysia, 11800 USM, Penang, Malaysia.

*Correspondence: sajadisa@student.usm.my

Received: 15 Aug 2025; Revised: 8 Sep 2025; Accepted: 18 Sep 2025; Published 30 Sep 2025

Abstract: Drought poses a significant threat to semi-arid regions such as Iran's Meighan Wetland, where limited ground-based data hinders effective monitoring and water resource management. This study addresses the challenge of assessing meteorological drought in data-scarce environments by integrating satellite-derived and reanalysis datasets with ground observations. The objective is to evaluate the spatiotemporal dynamics of drought in the Meighan Wetland from 1998 to 2025 using the Standardized Precipitation Index (SPI) and the Standardized Precipitation Evapotranspiration Index (SPEI) at 3-, 6-, and 12-month timescales. Monthly precipitation data from the GPM Final Run Version 7 and temperature data from the ERA5-Land product were validated against 10 synoptic stations, with six selected for detailed analysis due to their high accuracy ($R > 0.9$ for GPM, $R^2 > 0.98$ for ERA5-Land). Results identified major drought episodes in 2000, 2008, 2017, and 2021, with SPEI indicating greater severity due to rising evapotranspiration. Correlation between SPI and SPEI was strong ($R > 0.87$), particularly at longer timescales. Trend analysis using the Mann–Kendall test and Sen's slope estimator revealed significant drying trends in Arak during late winter and summer. This study demonstrates the efficacy of combining satellite and reanalysis data for robust drought monitoring, offering critical insights for adaptive water resource planning in semi-arid regions.

Keywords: GPM; ERA5-Land; Drought Indices; Time-series Analysis; Mann-Kendall Test

1.0 Introduction

Drought is a complex and pervasive natural hazard arising from prolonged periods of below-average precipitation, often leading to severe socio-economic and environmental consequences (Mishra & Singh, 2010, 2011). As one of the most recurrent and costly climate extremes, drought affects water availability, food production, energy supply, and ecosystem services. It is commonly classified into four major types: meteorological drought, defined by a precipitation deficit; hydrological drought, marked by reduced surface or subsurface water resources; agricultural drought, indicated by soil moisture deficiency and its impacts on crops; and socioeconomic drought, encompassing broader economic and social effects triggered by water shortages (Mishra & Singh, 2010; Wang et al., 2022).

In recent decades, numerous studies have emphasized that drought frequency, intensity, and spatial extent have increased under the influence of global climate change (Morid et al., 2006; Samantaray et al., 2022; Tan et al., 2022; Touma et al., 2015). This shift is particularly alarming in arid and semi-arid regions, where water scarcity is already critical and ecosystems are highly sensitive to hydroclimatic variability (Tan et al., 2017; Winkler et al., 2017). Effective drought monitoring requires continuous, high-quality climate data, yet in many developing regions, ground-based meteorological stations are sparse, unevenly distributed, and often suffer from discontinuities (García-Valdecasas Ojeda et al., 2021; Tan et al., 2017).

To address these limitations, satellite-based datasets and climate reanalysis products have become increasingly important in hydrometeorological research. Satellite-derived precipitation products such as the Tropical Rainfall Measuring Mission (TRMM) and the Global Precipitation Measurement (GPM) provide near-global coverage with high temporal and spatial resolution and have been widely applied in drought monitoring where dense observational networks are lacking (Chen et al., 2020; Tan et al., 2017). These datasets have proven useful across diverse regions, from East Africa (Naumann et al., 2012) to the Indian subcontinent (Kesarwani et al., 2023). However, validation studies have highlighted systematic biases in satellite precipitation estimates, particularly in mountainous or low-rainfall environments, underscoring the need for bias correction and validation against synoptic observations before operational application (Ashraf et al., 2022; De Jesús et al., 2016; Santos et al., 2017; Winkler et al., 2017).

In addition to precipitation, drought assessments increasingly require temperature information to quantify evaporative demand, which strongly influences drought severity (Pandey et al., 2021). ERA5-Land, a high-resolution global reanalysis dataset developed by the European Centre for Medium-Range Weather Forecasts (ECMWF), has emerged as a reliable source of hourly temperature and evapotranspiration data at 0.1° spatial resolution (Du et al., 2025; Torres-Vázquez et al., 2023; Ullah et al., 2021). ERA5-Land has been used to estimate potential evapotranspiration (PET) and to calculate temperature-sensitive drought indices such as the Standardized Precipitation Evapotranspiration Index (SPEI). Despite its consistency and coverage, ERA5-Land products should be validated locally to ensure regional accuracy.

For drought quantification, two widely used indices are the Standardized Precipitation Index (SPI) and the SPEI (Guttman, 1999; McKee et al., 1993). SPI, developed by McKee et al. (1993), measures drought solely based on precipitation anomalies and is effective across multiple timescales. SPEI, introduced by Vicente-Serrano et al. (2010), incorporates PET to capture both water supply and demand, making it particularly relevant in the context of global warming. These indices have been successfully applied worldwide to evaluate drought severity and duration, including in Iran (Lotfirad et al., 2022), Algeria (Haied et al., 2017), Europe (Spinoni et al., 2015), and China (Jain et al., 2015).

To analyze drought evolution over time, non-parametric statistical methods such as the Mann–Kendall (MK) test and Sen's slope estimator are widely used. The MK test identifies monotonic trends in time series data without requiring assumptions about normality or linearity, while Sen's slope quantifies the rate of change. These methods have been applied extensively to detect changes in precipitation, temperature, and drought indices across diverse climates (Chen et al., 2020; Irannezhad et al., 2016; Liu et al., 2021).

In this study, I aim to evaluate the spatiotemporal dynamics of meteorological drought in and around the Meighan Wetland of Iran, a sensitive hydrological system located in a semi-arid region where water stress has ecological and socio-economic implications. The research integrates ground-based synoptic observations with GPM precipitation and ERA5-Land temperature data, applying SPI and SPEI at multiple timescales. Dataset validation, characterization of drought frequency and severity, and trend detection form the core of this analysis.

The specific objectives of this study are to:

- Validate GPM and ERA5-Land datasets against synoptic station data.
- Assess the spatiotemporal variability of drought using SPI and SPEI at 3-, 6-, and 12-month scales.
- Classify and quantify drought characteristics (frequency, intensity, duration).
- Analyze long-term drought trends using Mann–Kendall and Sen's slope methods.
- Provide insights for improving drought monitoring and regional water resource planning.

Journal of Asian Geography, 2025, Volume 4 (Issue 2), 46-62
https://doi.org/10.36777/jag2025.4.2.6

2.0 Study Area

The Meighan Wetland is located in central Iran, within Markazi Province, and spans between 33°49′29″ to 34°44′52″ N latitude and 49°22′13″ to 50°17′55″ E longitude. It lies in a closed basin situated between the Zagros Mountains to the west and the Central Iranian Mountains to the east, covering an area of about 545,229 hectares. The watershed consists of eight main sub-basins—Karahrud, Mehrabad, Saruq, Shahrab, Ashtian, Ebrahimabad, Kheirabad, and Amanabad—and lacks any perennial rivers. Approximately 65% of the area (about 353,800 hectares) is composed of plains, while the remainder consists of hills and mountainous terrain.

At the center of the watershed lies Meighan Salt Lake, a seasonal saline wetland of high ecological significance that is particularly vulnerable to both climatic variability and human pressures. The lake and its surroundings feature diverse geomorphological landscapes, including halophyte-covered lands, dunes, alluvial fans, and flat plains. These characteristics, coupled with the region's closed hydrological system, make Meighan an important site for studying drought in semi-arid environments.

Climatically, the region receives an average annual precipitation of around 287 mm (Regional Water Company of Markazi, RWCM). Long-term records from the Arak meteorological station indicate an average annual temperature of about 14 °C, with historical extremes ranging from −30.5 °C to +44 °C. Evaporation is high, reaching up to 2,036 mm per year, contributing to persistent water stress. The area also experiences a prolonged dry season lasting about 150 days, from early June to early November, during which relative humidity drops as low as 28%. In contrast, winter months are more humid, with average relative humidity around 63%. Overall, the annual average relative humidity is about 46%, and total annual sunshine reaches nearly 2,993 hours (Department of Environment, DOE).

For this study, data from 10 synoptic meteorological stations were utilized: Arak, Tafresh, Khomeyn, Komijan, Mahallat, Shazand, Salafchegan, Delijan, Avaj, and Dorud. Their geographic distribution spans a range of elevations and climatic conditions across the watershed, and these stations were critical in validating satellite-derived datasets. Figure 1 presents an overview of the study area, including the location of the Meighan Wetland, the Digital Elevation Model (DEM), and the positions of the meteorological stations.

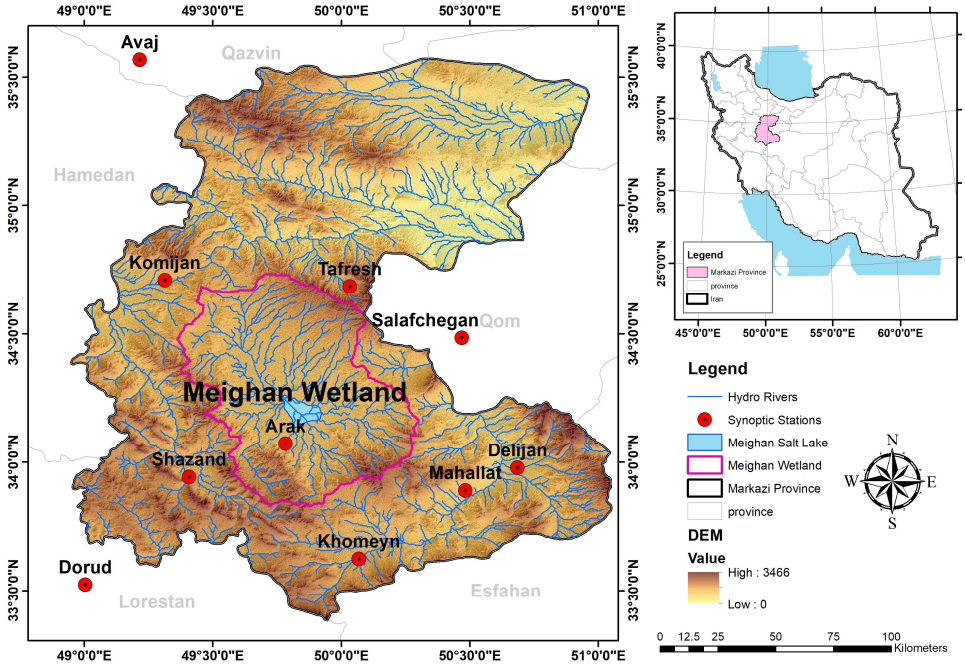

Figure 1: Location of the Meighan Wetland in central Iran.

3.0 Materials and Methodology

3.1 Precipitation Data

This study uses monthly precipitation data from the Global Precipitation Measurement (GPM) mission, specifically the Integrated Multi-satellite Retrievals for GPM (IMERG) Final Run Version 7 product. The GPM mission, jointly developed by NASA and JAXA, provides high-resolution, satellite-based precipitation estimates with near-global coverage (60°N–60°S). The IMERG Final Run integrates data from multiple sensors and applies gauge-based bias correction, making it well-suited for retrospective drought analysis. The dataset has a spatial resolution of 0.1° (~10 km) and a temporal resolution of 30 minutes, but for this study it was aggregated to monthly values for the period 1998–2025.

In addition to satellite data, daily ground-based precipitation records from 10 synoptic stations were obtained from the Iranian Meteorological Organization. These stations—Arak, Tafresh, Khomeyn, Komijan, Mahallat, Shazand, Salafchegan, Delijan, Avaj, and Dorud—are distributed across Markazi Province and were selected for their record length and continuity. Their locations span diverse topographic and climatic zones within the basin, enabling representative validation of the satellite dataset. Daily precipitation observations were aggregated to monthly totals to align with the GPM data. Table 1 summarizes each station's characteristics, including geographic coordinates, elevation, and data availability period.

Journal of Asian Geography, 2025, Volume 4 (Issue 2), 46-62
https://doi.org/10.36777/jag2025.4.2.6

Table 1: Synoptic meteorological stations used for precipitation validation in the Meighan Wetland

No	Name	Longitude	Latitude	Elevation	From	To
1	Arak	49.783333	34.071944	1702.8	2000	June 2022
2	Tafresh	50.033333	34.684444	1979.7	2001	June 2022
3	Khomeyn	50.069167	33.623889	1834.6	2001	June 2022
4	Komijan	49.314444	34.709722	1741	2005	June 2022
5	Mahallat	50.483333	33.888889	1622	2006	June 2022
6	Shazand	49.408333	33.941667	1913	2010	June 2022
7	Salafchegan	50.469444	34.483611	1381.4	2003	June 2022
8	Delijan	50.686111	33.977222	1524.3	2003	June 2022
9	Avaj	49.2167	35.5667	2034.9	2000	June 2022
10	Dorud	49.004444	33.523611	1522.3	2000	June 2022

3.2 Temperature Data

The temperature data used in this study were obtained from the ERA5-Land reanalysis dataset, developed by the European Centre for Medium-Range Weather Forecasts (ECMWF). ERA5-Land provides hourly data at a spatial resolution of 0.1° (~9 km), offering greater detail over land areas compared to the standard ERA5 product. Its fine spatial and temporal resolution, combined with consistent long-term coverage, makes it a valuable resource for climate analysis, particularly in data-scarce or topographically complex regions such as central Iran

For this research, monthly averages of minimum, maximum, and mean temperature were extracted from ERA5-Land for the period 1998–2025. Complementary ground-based temperature data were obtained from 10 synoptic meteorological stations, which provided daily records of minimum, maximum, and mean temperature. These daily observations were aggregated to monthly averages to match the temporal resolution of the ERA5-Land dataset.

Over the study period, the seasonal temperature cycle in the region is clear and consistent. Summers are typically hot and dry, with July and August recording the highest average temperatures, while January represents the coldest period (Figure 2). These seasonal patterns, observed in both the reanalysis and ground-based datasets, highlight the semi-arid climate of central Iran and underscore the importance of temperature–precipitation interactions in shaping drought dynamics within the basin.

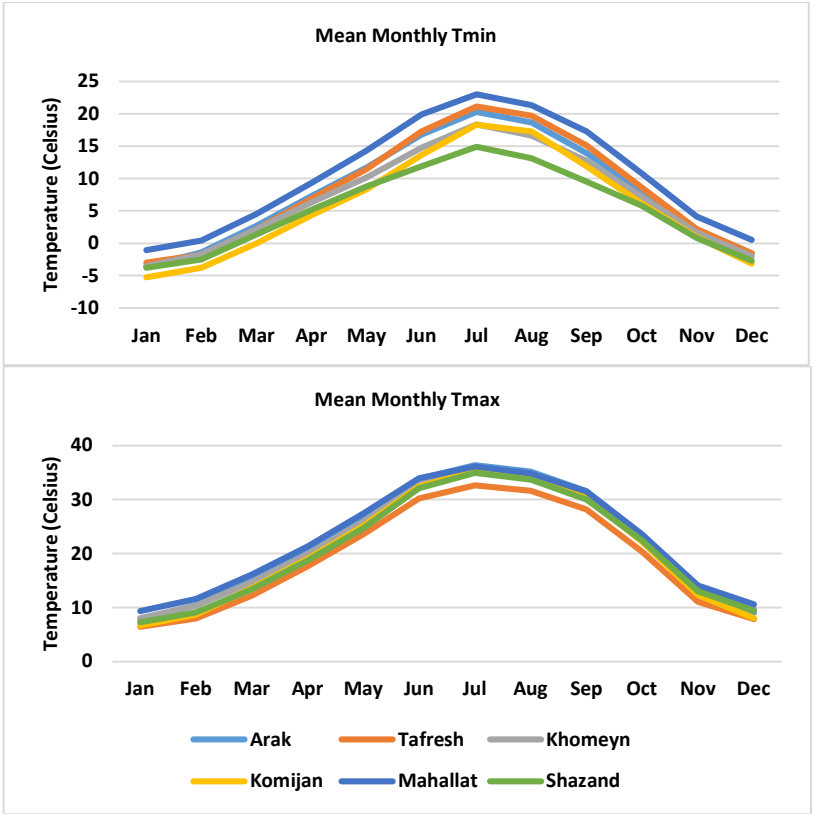

Figure 2: Monthly Minimum and maximum temperature trends based on synoptic observations.

3.3 Validation Process and Statistical Analysis

To ensure the reliability of GPM precipitation and ERA5-Land temperature data for drought monitoring in the Meighan Wetland, both datasets were validated against observations from 10 synoptic stations (Arak, Tafresh, Khomeyn, Komijan, Mahallat, Shazand, Salafchegan, Delijan, Avaj, and Dorud) for the period 2000–2022, depending on data availability. A point-to-pixel validation approach was applied, in which each station's precipitation time series was directly compared with the corresponding GPM grid cell, thereby minimizing interpolation errors and

ensuring location-specific accuracy. Dataset performance was evaluated using the Pearson correlation coefficient (R), root mean square error (RMSE), and relative bias, with the statistical framework summarized in Table 2.

Table 2: Statistical Metrics (T = TRMM, O = Synoptic Observed Data)

Methods/Unit	Equation
Root Mean Square Error (RMSE)/mm	$RMSE = \sqrt{\frac{1}{n}\sum_{i=1}^{n}(T_i - O_i)^2}$
Pearson Linear Correlation Coefficient (R)	$R = \frac{\sum_{i=1}^{n}(O_i-\overline{O})(T_i-\overline{T})}{\sqrt{\sum_{i=1}^{n}(O_i-\overline{O})^2}\cdot\sqrt{\sum_{i=1}^{n}(T_i-\overline{T})^2}}$
Relative Bias (Bias)/%	$Bias = \frac{\sum_{i=1}^{n}(T_i-O_i)}{\sum_{i=1}^{n}O_i}(100)$

GPM precipitation correlated strongly with stations such as Arak, Khomeyn, and Shazand (R > 0.9); however, systematic biases were observed, with overestimation at arid lowland stations (Salafchegan, Delijan; Bias > +45%) and underestimation at high-elevation sites (Avaj, Dorud; negative Bias). ERA5-Land temperature showed excellent agreement across all stations (R ⩾ 0.98, with low RMSE and Bias), confirming its suitability for drought analysis. Station-by-station performance is provided in Table 3, and the spatial distribution of GPM reliability across the study area is illustrated in Figure 3. Based on these results, the six stations with the highest accuracy and closest proximity to the Meighan Wetland (Arak, Tafresh, Khomeyn, Komijan, Mahallat, and Shazand) were selected to calculate mean precipitation across the wetland (2011–2021) and to perform seasonal assessments, while Salafchegan, Delijan, Avaj, and Dorud were excluded due to significant biases or spatial mismatches.

Table 3: Statistical Analysis

Synoptic Stations	Date		Years	GPM Data			ERA5-Land Data		
	Start	End		RMSE (mm/month)	Bias %	R	RMSE (mm/month)	Bias %	R
Arak	2000	2022	20	15	33.6	0.94	1.2	-5.6	0.99
Tafresh	2001	2022	19	10.9	5.8	0.91	3.6	-24.1	0.99
Khomeyn	2001	2022	19	14.6	33.7	0.94	2.6	-14.6	0.99
Komijan	2005	2022	15	14.8	36.7	0.93	2.1	-12.3	0.99
Mahallat	2006	2022	14	12.3	42.4	0.92	2.8	-14.6	0.99
Shazand	2010	2022	10	14.9	0.9	0.93	2.6	-13.8	0.98
Salafchegan	2003	2022	17	11.3	46.2	0.92	1.7	-7.8	0.99
Delijan	2003	2022	17	11.5	47.2	0.92	1.4	-4.7	0.99
Avaj	2000	2022	20	14.5	-6.8	0.89	2.8	-20.4	0.98
Dorud	2000	2022	20	25	-1.9	0.91	3.9	-21.6	0.99

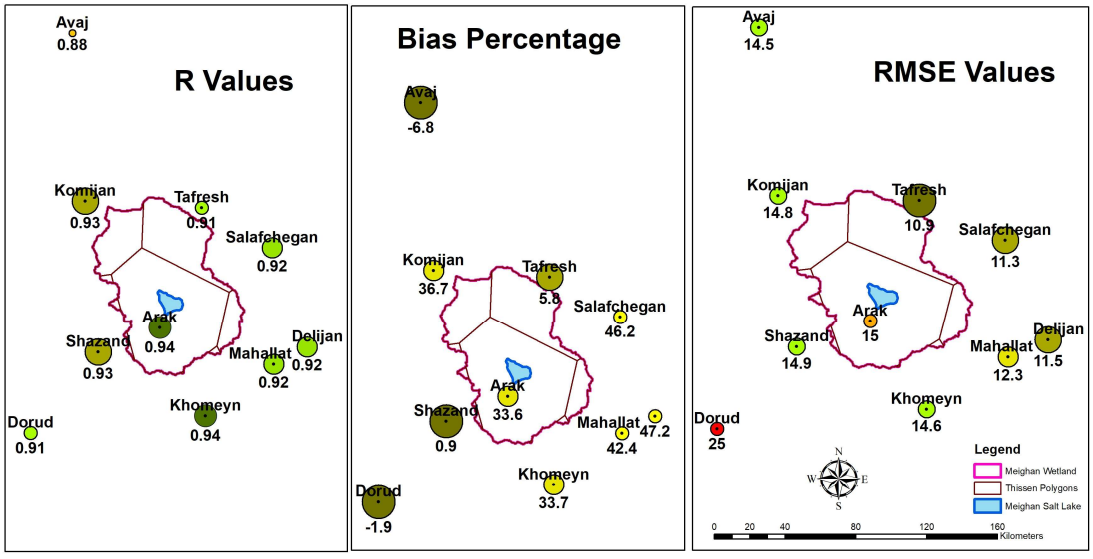

Figure 3: Spatial distribution of Statistical Metrics in 10 Point-to-Pixel Locations (Comparing GPM Final-Run data with 10 Synoptic Stations' Precipitation Data)

To estimate precipitation across the wetland, the Thiessen polygon method was first applied to calculate monthly areal mean precipitation, weighting each station according to its area of influence (Figure 4). This approach ensured an accurate representation of station contributions within a sparse network. The resulting Thiessen polygons are shown in Figure 5. For spatial visualization, Inverse Distance

Journal of Asian Geography, 2025, Volume 4 (Issue 2), 46-62
https://doi.org/10.36777/jag2025.4.2.6

Weighting (IDW) was then employed to generate continuous precipitation surfaces, capturing gradual variability across the wetland (Figure 6). Together, Thiessen polygons provided quantitative accuracy for areal averages, while IDW offered interpretable spatial patterns, enhancing both the reliability and presentation of precipitation estimates.

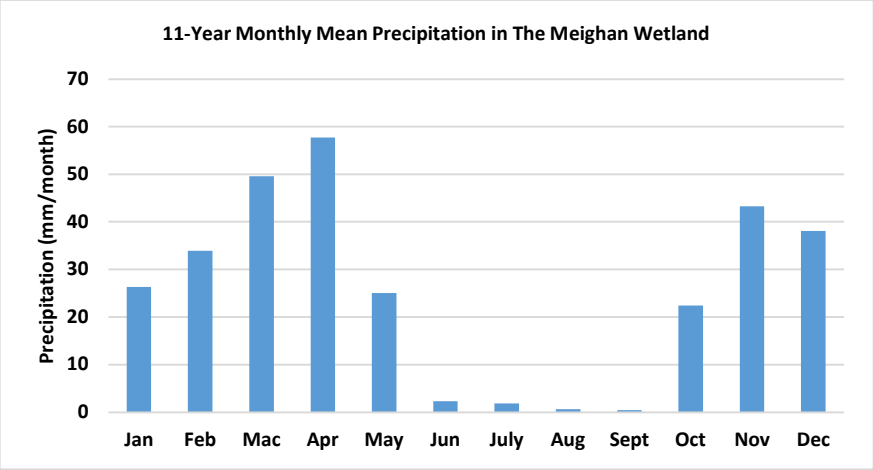

Figure 4: Monthly Mean Precipitation of the Meighan Wetland from 2011 to 2021.

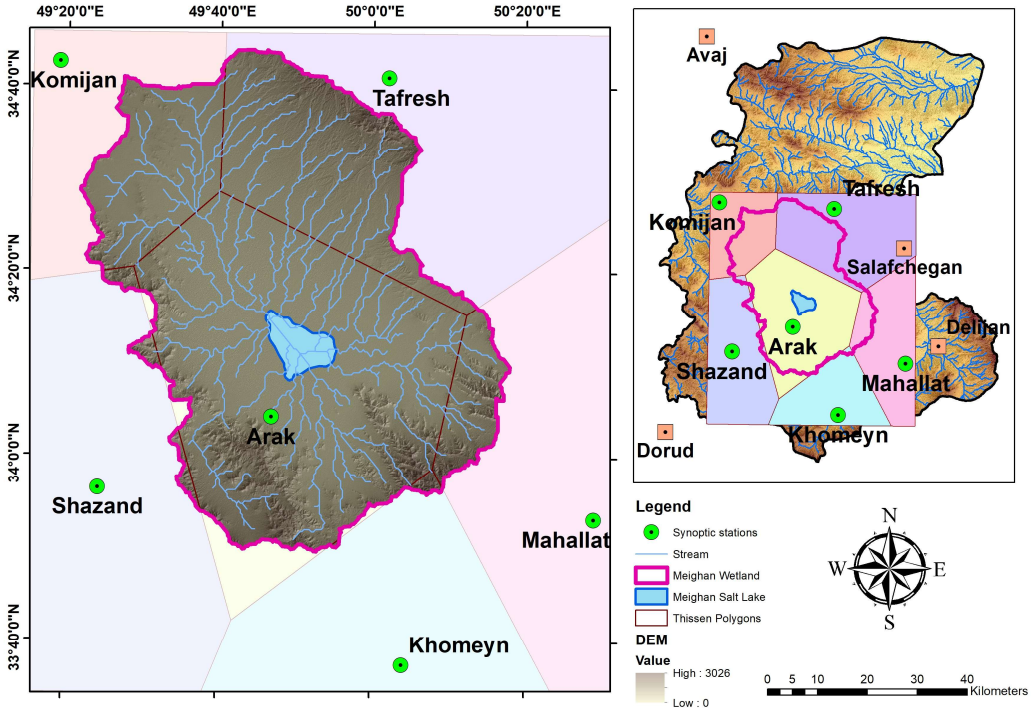

Figure 5: Thiessen Polygon Method Conducted for Meighan Wetland Area

Seasonal validation of GPM data (2011–2021) using the six selected stations revealed the highest agreement in autumn (R = 0.94, low RMSE) and spring (R = 0.87), with weaker performance in summer (R = 0.71) due to sparse convective rainfall. Winter showed moderate agreement (R = 0.85) but higher bias (+35.6%), particularly in areas influenced by frontal rainfall. These seasonal results are presented in Figures 6 and 7. The findings are consistent with similar studies in other semi-arid and monsoon-influenced basins, such as the Kelantan River Basin in Malaysia (Tan et al., 2017), where satellite precipitation retrievals also exhibited limitations in capturing convective rainfall.

Journal of Asian Geography, 2025, Volume 4 (Issue 2), 46-62
https://doi.org/10.36777/jag2025.4.2.6

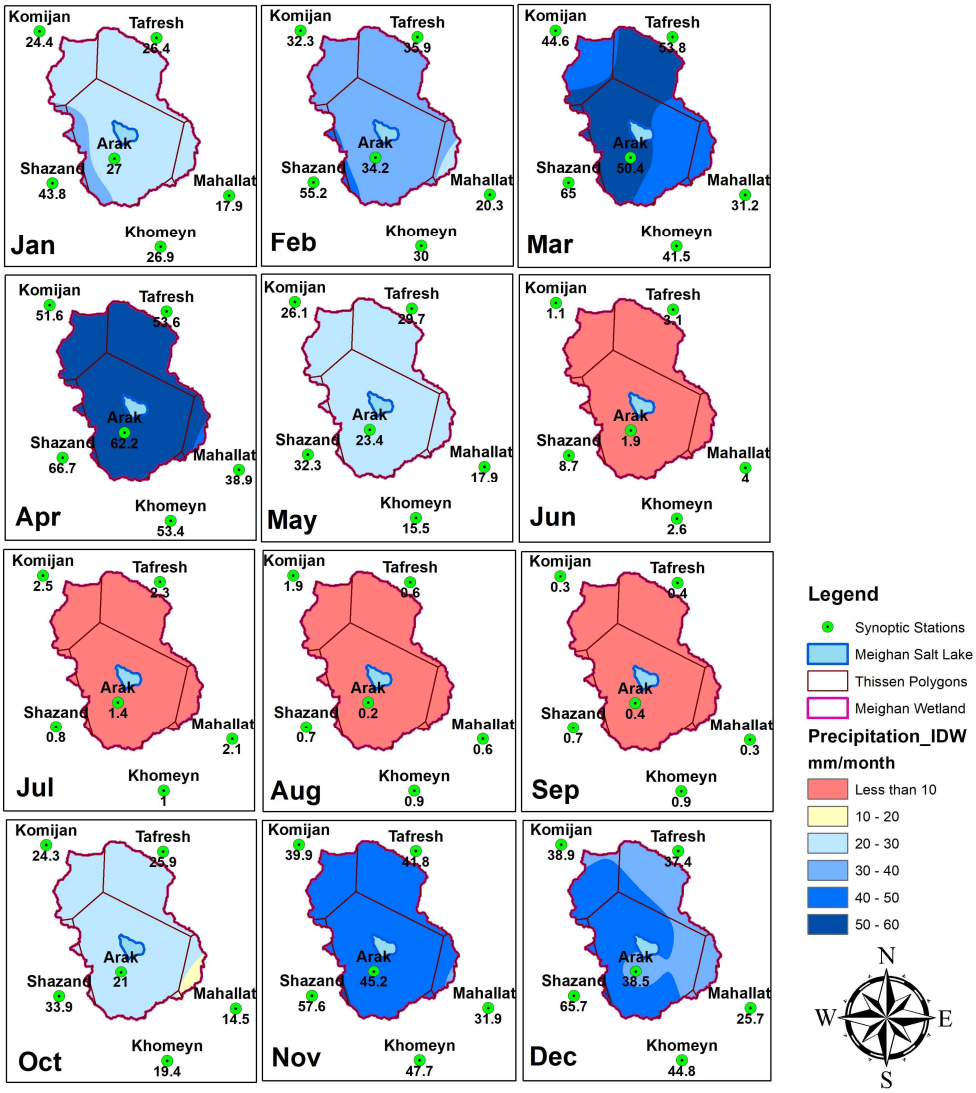

Figure 6: Precipitation Distribution across the Meighan Wetland

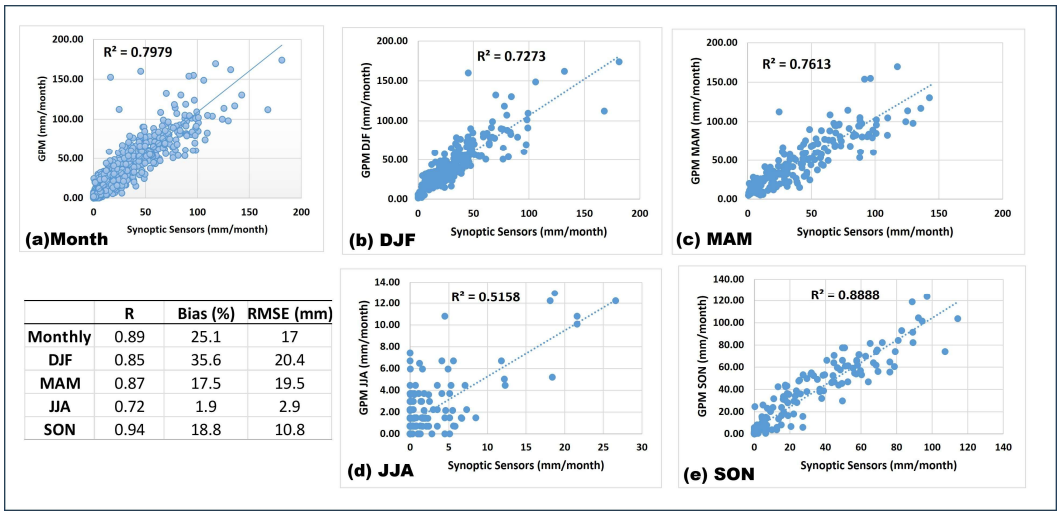

	R	Bias (%)	RMSE (mm)
Monthly	0.89	25.1	17
DJF	0.85	35.6	20.4
MAM	0.87	17.5	19.5
JJA	0.72	1.9	2.9
SON	0.94	18.8	10.8

Figure 7: Scatter plots of (a) monthly, (b) December to February, (c) March to May, (d) June to August, and (e) September to November seasonal precipitation derived from the GPM and Synoptic Observation in 2011-2021

3.4 Standardized Precipitation Index (SPI)

The SPI is a widely used meteorological index for assessing drought conditions based on precipitation data. Developed by McKee et al. (1993), SPI is calculated by fitting observed precipitation to a probability distribution, such as the Gamma or Pearson Type III distribution. The index quantifies the deviation of precipitation from the long-term average over a specific period. Being "standardized" allows for comparison of drought conditions across different climates (e.g., deserts versus rainforests). SPI can be computed at multiple timescales (e.g., 1-, 3-, 6-, and 12-month) to capture short-term or long-term drought conditions. SPI values range from −3 to +3, where positive values indicate wetter-than-average conditions and negative values indicate drier-than-average conditions (Table 4).

Table 4: Standardized Precipitation Index (SPI) Classification:

Class	SPI Value
Extremely Wet	SPI ≥ 2
Severely Wet	1.5 ≤ SPI < 2
Moderately Wet	1 ≤ SPI < 1.5
Near-Normal	-1 < SPI < 1
Moderately Dry	-1.5 < SPI ≤ -1
Severely Dry	-2 < SPI ≤ -1.5
Extremely Dry	SPI ≤ -2

In this study, SPI was calculated at 3-, 6-, and 12-month timescales to capture different aspects of drought. The 3-month SPI (SPI-3) represents short-term, seasonal precipitation deficits relevant to agriculture and ecosystems; the 6-month SPI (SPI-6) reflects medium-term hydrological stress; and the 12-month SPI (SPI-12) captures long-term changes in water balance that affect groundwater recharge and wetland dynamics. While results were generated for all three timescales, drought characteristics such as duration, severity, frequency, and intensity, and trend analyses primarily focused on SPI-3, as short-term droughts are most critical for the Meighan Wetland's agricultural and ecological systems.

3.5 Standardized Precipitation Evapotranspiration Index (SPEI)

The Standardized Precipitation Evapotranspiration Index (SPEI), introduced by Vicente-Serrano et al. (2010), is a widely used drought index that incorporates the effects of both precipitation and temperature. Unlike SPI, which relies solely on precipitation, SPEI accounts for potential evapotranspiration (PET), making it particularly suitable for assessing drought under changing climatic conditions. The index is calculated by fitting the monthly climatic water balance (precipitation minus PET) to a log-logistic distribution, which is then standardized to produce values comparable to a normal distribution.

In this study, SPEI was calculated at 3-, 6-, and 12-month timescales using precipitation from the GPM IMERG Final Run V7 and PET derived from ERA5-Land temperature inputs via the Thornthwaite method. SPEI-3 reflects short-term seasonal drought variability, SPEI-6 captures medium-term water stress, and SPEI-12 highlights long-term drought evolution. Similar to SPI, SPEI-3 was emphasized in drought characteristics and trend analyses, as short-term droughts have the most immediate impacts on agriculture, water resources, and wetland ecosystems in the region.

3.6 Potential Evapotranspiration (PET)

Potential evapotranspiration (PET) represents the atmospheric demand for moisture and is a key variable in drought analysis, particularly in semi-arid and arid regions. It reflects the amount of water that would be evaporated and transpired by vegetation if sufficient water were available. In this study, PET was incorporated into the SPEI calculation to account for temperature-driven drought stress.

Monthly PET values were estimated using the Thornthwaite method, which calculates evapotranspiration based on average monthly temperature and latitude. While less detailed than energy-based models such as Penman–Monteith, the Thornthwaite method is widely used due to its simplicity and minimal data requirements, especially when only temperature data are available. Temperature inputs for PET were derived from the ERA5-Land reanalysis dataset for the period 1998–2025, providing spatially continuous and climatologically robust estimates of evapotranspiration across the Meighan Wetland watershed.

3.7 Drought Characteristics

To better understand the nature and impacts of drought events in the Meighan Wetland region, several drought characteristics (DC) were extracted from the SPI-3 time series. These characteristics describe not only the frequency of droughts but also their intensity and duration, providing a more comprehensive view of drought dynamics beyond single-month anomalies. The main parameters analyzed include:

- Drought Duration: the number of consecutive months during which SPI values remain below zero.
- Drought Intensity: the cumulative severity of a drought event, typically measured as the sum of SPI values over the drought period.
- Drought Magnitude: the absolute value of the sum of negative SPI values during a drought event.
- Drought Frequency: the total number of drought events observed over the study period.

3.8 Trend Analysis Using Mann-Kendall and Sen's Slope Estimator

To evaluate long-term drought dynamics in the Meighan Wetland region, trend analyses were performed on the SPI-3 and SPEI-3 time series using a combined non-parametric approach. The Mann–Kendall (MK) test, developed by Mann (1945) and later refined by Kendall (1975), was employed to detect the presence and direction of monotonic trends, while Sen's slope estimator was applied to quantify their magnitude. The MK test is particularly suitable for hydrological and climatic data because it can detect trends without assuming normality or linearity. A positive Z-value from the MK test indicates an increasing trend (wetting), whereas a negative Z-value signifies a decreasing trend (drying). Trend significance was evaluated at the 90%, 95%, and 99% confidence levels using the standard normal distribution. The MK test was conducted using the MAKESENS program, which simplifies the computation of Z-values and supports graphical interpretation. This method has been widely applied in regional drought assessments (Khanmohammadi et al., 2022; Tuan & Canh, 2021).

Sen's slope estimator, a non-parametric method introduced by Sen (1968), calculates the median of all possible pairwise slopes between data points in a time series, providing a robust measure of the rate of change. A positive slope indicates a trend toward wetter conditions, while a negative slope represents increasing drought severity. The estimator is resistant to outliers and is widely used to identify gradual, consistent changes in climate variables. It has been extensively applied in drought trend studies across Asia and the Middle East, particularly in semi-arid climates. By integrating the MK test and Sen's slope estimator, this study provides a comprehensive framework for analyzing

drought trends, capturing both the presence and direction of trends, as well as their magnitude and intensity in precipitation-driven (SPI-3) and temperature-sensitive (SPEI-3) drought conditions.

4.0 Results and Discussion

4.1 Spatio-temporal Changes in Precipitation

The annual precipitation trends from 1998 to 2025 across the six selected stations, Arak, Tafresh, Khomeyn, Komijan, Mahallat, and Shazand show considerable interannual variability in rainfall patterns (Figure 8). Although no consistent upward or downward trend is visually dominant over the period, some notably dry years stand out, including 2000, 2008, and 2021, when total annual precipitation fell below 300 mm at most stations. In contrast, 2004 and 2015 recorded peak rainfall exceeding 450 mm at stations such as Arak and Shazand. Among the six stations, Shazand consistently recorded the highest annual rainfall, while Mahallat and Tafresh remained relatively dry. This spatial heterogeneity indicates that even within the relatively compact Meighan watershed, topographic influences and localized climatic effects play a significant role in precipitation distribution.

The mean monthly precipitation patterns (Figure 8) exhibit a typical semi-arid seasonal distribution, with most rainfall occurring between November and April. Peak rainfall is observed in March and April, followed by a sharp decline during late spring. From June to September, all stations experience minimal rainfall, often below 5 mm/month, reflecting the region's prolonged dry season. This dry period, coinciding with high temperatures and elevated evapotranspiration, highlights the Meighan Wetland's vulnerability to seasonal drought stress. The monthly cycle is generally consistent across the six stations, though some variation in intensity exists; for example, Shazand typically receives more precipitation in March–April, whereas Mahallat generally lags slightly in peak totals. These observations provide essential seasonal context for understanding SPI and SPEI dynamics in the region.

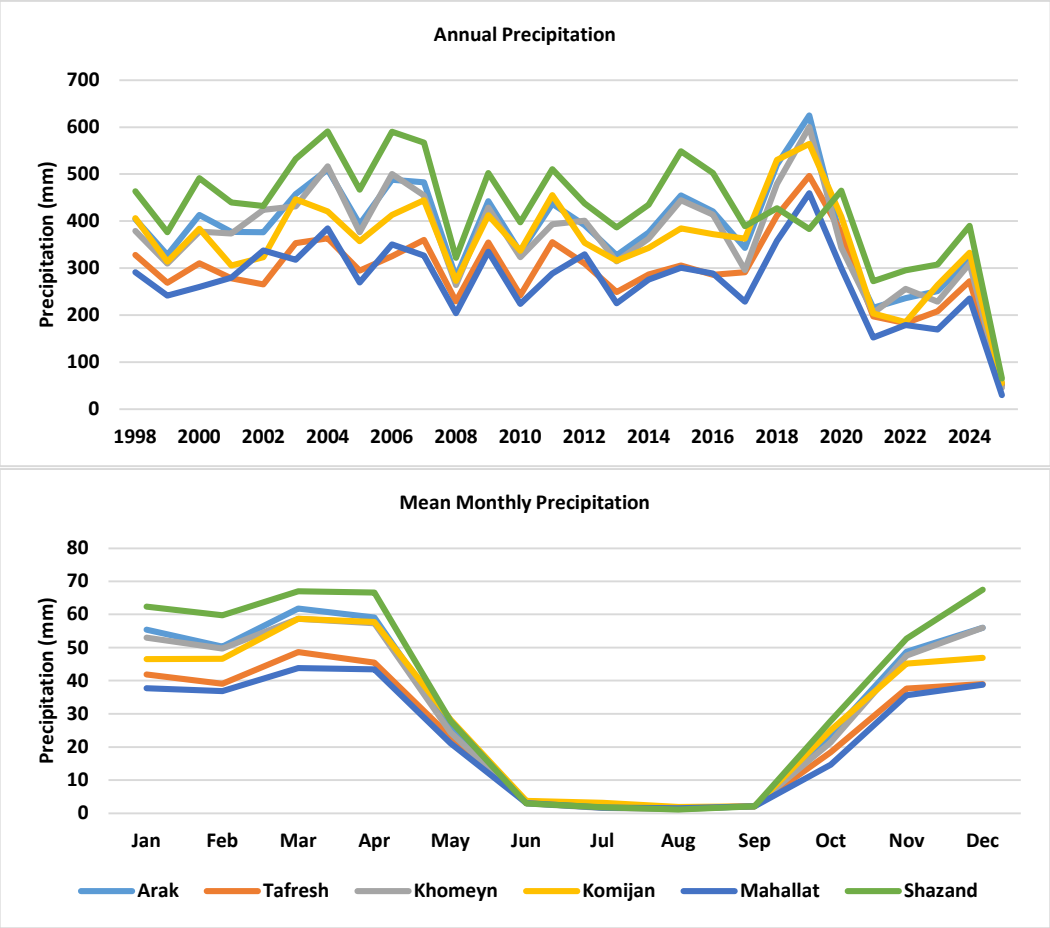

Figure 8: Annual and Mean Monthly Precipitation (1998-2025)

4.2 Comparison of SPI-3 and SPEI-3 derived from Synoptic and Satellite Data

To evaluate the consistency between satellite-based and ground-observed drought indices, SPI-3 and SPEI-3 values derived from GPM and ERA5-Land were compared with those calculated from synoptic station data at the six validated stations: Arak, Tafresh, Khomeyn, Komijan, Mahallat, and Shazand.

Figure 9 presents the comparison between the SPI-3 time series computed from GPM and those based on synoptic observations. The results show generally high agreement across all stations. The strongest correlations were found at Arak (R = 0.88) and Khomeyn (R = 0.87), followed closely by Mahallat (R = 0.84) and Tafresh (R = 0.83). Moderate agreement was observed at Shazand (R = 0.81) and Komijan (R = 0.78). These results confirm that SPI-3 calculated from GPM Final Run V7 closely follows observed drought patterns in both timing and intensity.

Journal of Asian Geography, 2025, Volume 4 (Issue 2), 46-62
https://doi.org/10.36777/jag2025.4.2.6

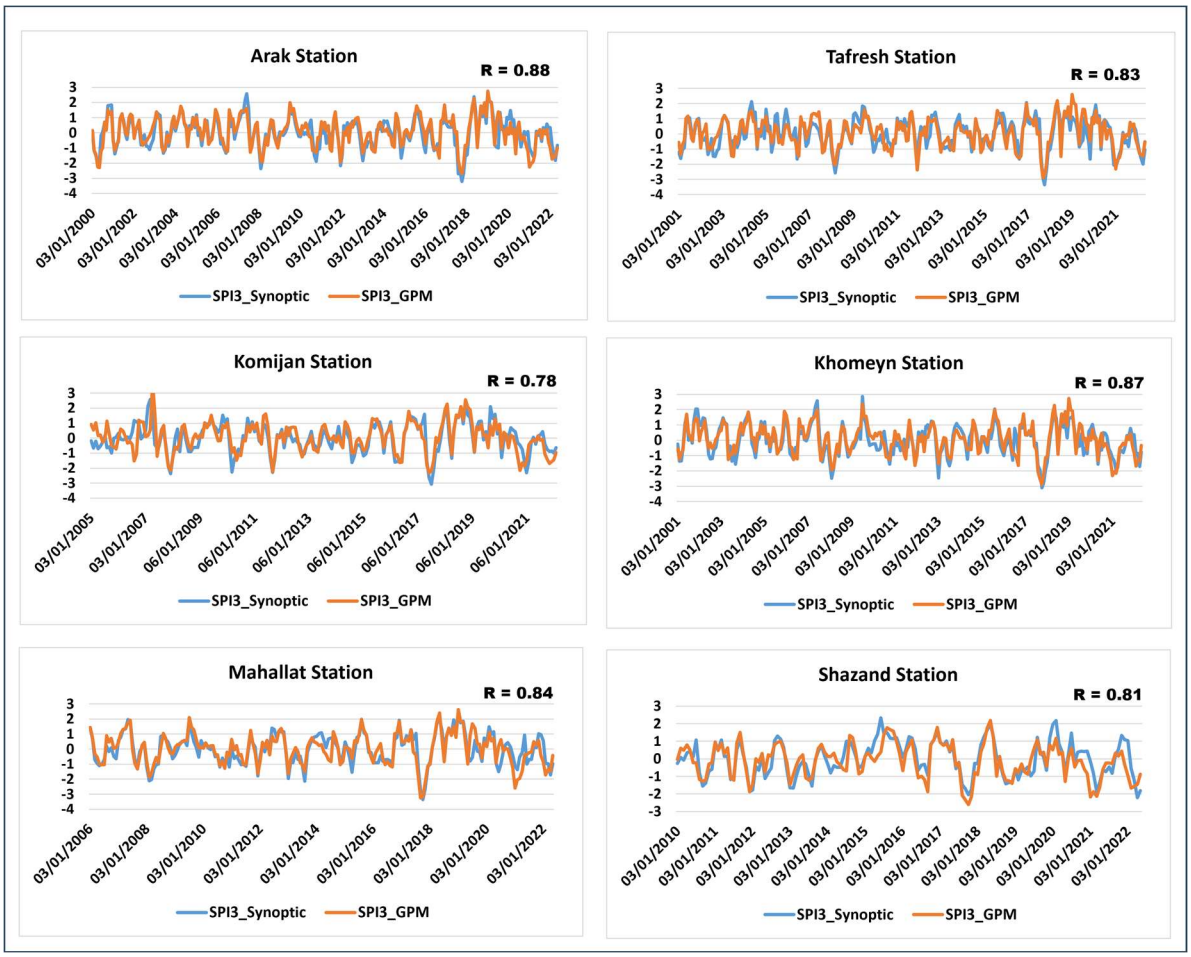

Figure 9: SPI-3 Derived from GPM and Synoptic Precipitation Inputs

In Figure 10, the comparison of SPEI-3—derived from GPM precipitation and ERA5-Land temperature inputs with synoptic-based values also demonstrates encouraging consistency. The strongest agreement was observed at Tafresh (R = 0.85) and Khomeyn (R = 0.83). Other stations, such as Komijan (R = 0.80) and Mahallat (R = 0.76), showed acceptable correlations. Shazand, however, exhibited a weaker match (R = 0.72), possibly due to higher local variability in temperature and evapotranspiration affecting PET estimation. The Arak value could not be directly retrieved due to formatting issues but was visually interpreted from the figure to be above 0.80.

Overall, the side-by-side comparison confirms that both SPI-3 and SPEI-3 derived from satellite-based sources reasonably replicate observed drought patterns. This supports the use of these datasets for drought monitoring in areas with sparse ground station coverage, particularly for operational early warning systems and long-term climate impact assessments.

Journal of Asian Geography, 2025, Volume 4 (Issue 2), 46-62
https://doi.org/10.36777/jag2025.4.2.6

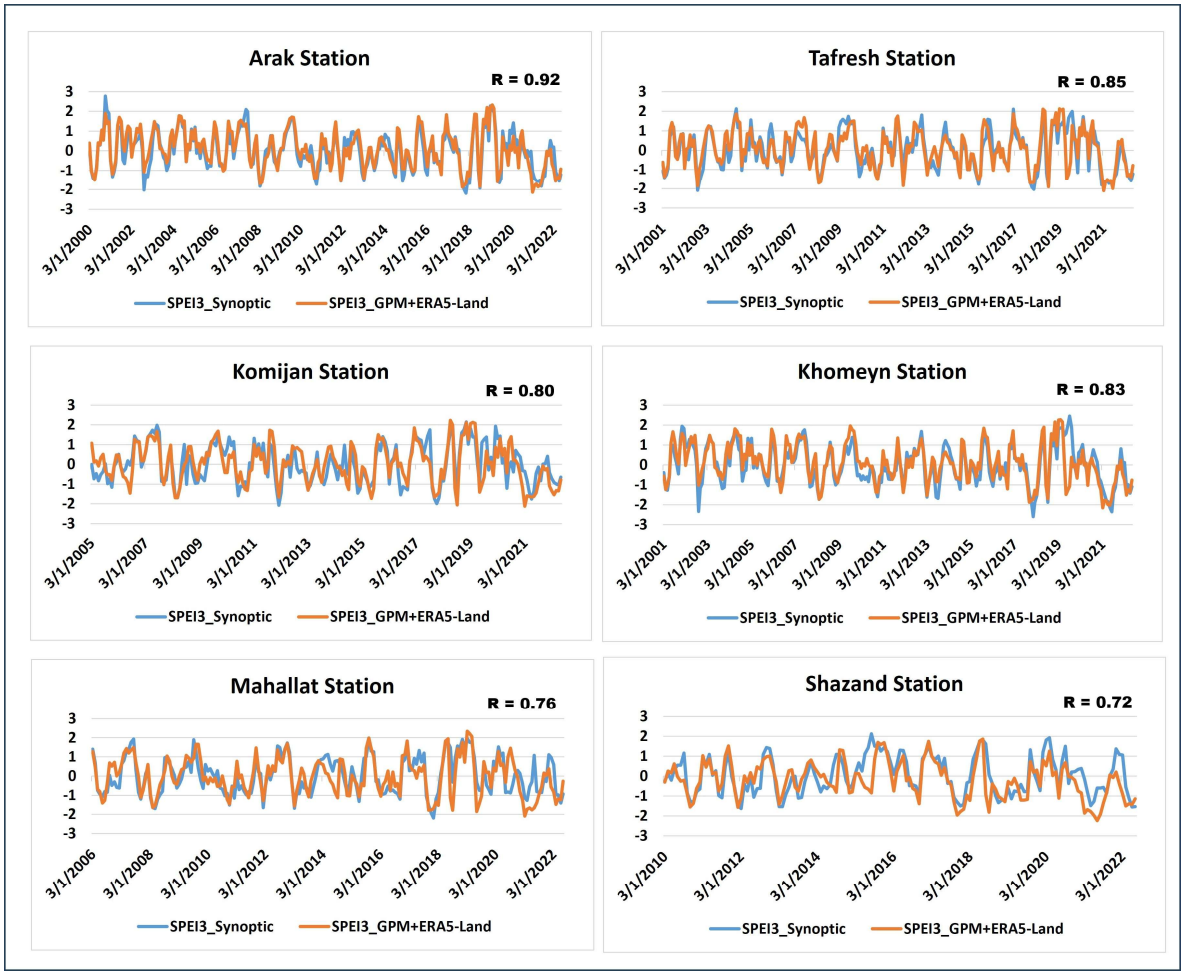

Figure 10: SPEI-3 Derived from Satellite-based and Synoptic Precipitation Inputs

4.3 Assessment of Meteorological Drought Using SPI and SPEI

To assess meteorological drought at different temporal scales, SPI and SPEI were calculated at 3-, 6-, and 12-month intervals using GPM and ERA5-Land data. This approach provides insight into both short-term water stress and long-term drought development across the six validated stations: Arak, Tafresh, Khomeyn, Komijan, Mahallat, and Shazand.

As shown in Figure 11, which presents SPI and SPEI results for Tafresh and Komijan, frequent short-term droughts are evident in the SPI-3 and SPEI-3 series, particularly during 2000, 2008, 2017, and 2021. In Komijan, both indices fell below −2 in 2008 and 2021, indicating episodes of extreme short-term drought. Tafresh experienced a sharp but brief event in 2018, with SPEI-3 reaching approximately −1.9. At the 6-month timescale, drought intensity in both stations remained significant during 2000–2001 and 2017, reflecting seasonal-to-half-year water deficits. SPEI-6 values in Komijan during mid-2017 dropped to around −2.1, suggesting persistent atmospheric drought conditions likely driven by rising temperatures.

Figure 12 displays the SPI and SPEI curves for Khomeyn and Shazand. Similar to the other stations, both showed strong short- and medium-term drought signals in 2000, 2008, 2017, and 2021. In Shazand, SPEI-3 fell below −2.0 in spring 2021, indicating a sharp seasonal drought likely linked to both rainfall shortage and high PET. Khomeyn experienced consistent declines in SPI-6 and SPEI-6 during 2000 and 2017, with moderate-to-severe drought categories sustained for several months. These patterns confirm the spatial consistency of drought episodes across the watershed.

The 12-month SPI and SPEI series, visible across both figures, provide a longer-term perspective on drought evolution. The 2000–2001 drought is clearly evident across all four stations, with SPEI-12 in Komijan dropping below −2.2 by late 2001. In Tafresh, the 2017–2018 event marked a significant but not extreme drought, with SPEI-12 reaching −1.71 in March 2018. Shazand and Khomeyn exhibited similar long-term declines during 2008 and 2021, though the magnitude mostly remained within the moderate-to-severe range. These longer timescales emphasize the persistence and accumulation of drought conditions, which are critical for understanding hydrological impacts on groundwater and wetland systems.

Taken together, SPI and SPEI assessments across multiple timescales confirm that 2000, 2008, 2017, and 2021 were the most impactful drought years in the region. SPEI consistently reported lower values than SPI in several instances, reflecting the added influence of rising temperatures and evapotranspiration on drought severity.

Journal of Asian Geography, 2025, Volume 4 (Issue 2), 46-62
https://doi.org/10.36777/jag2025.4.2.6

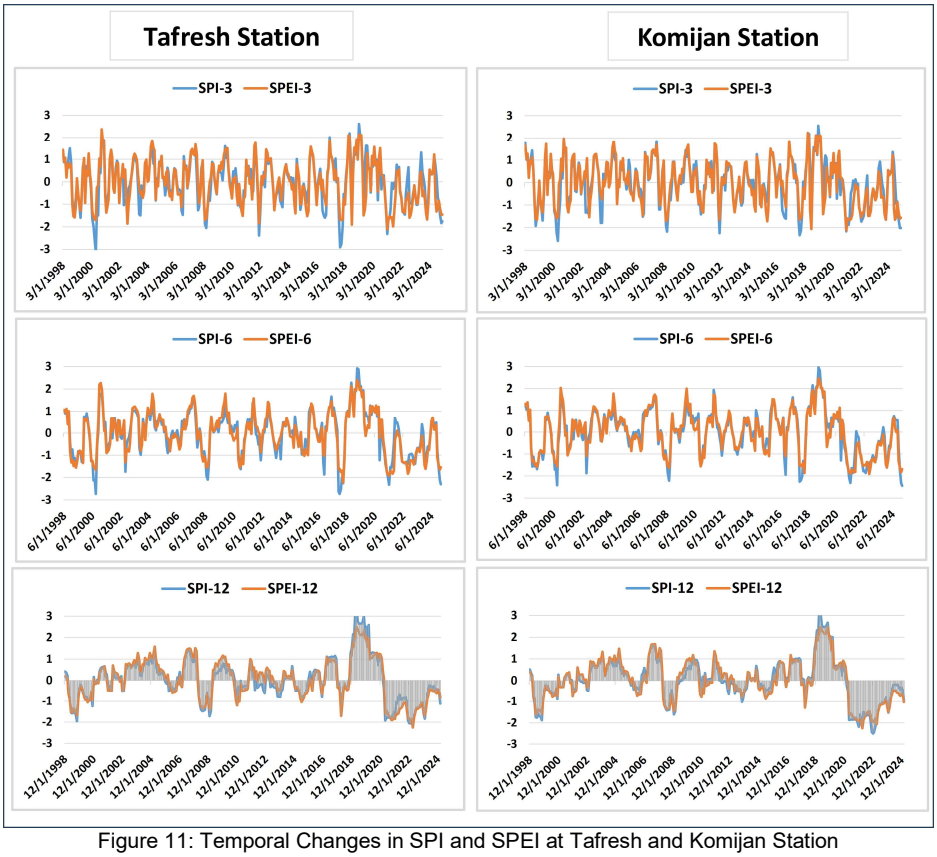

Figure 11: Temporal Changes in SPI and SPEI at Tafresh and Komijan Station

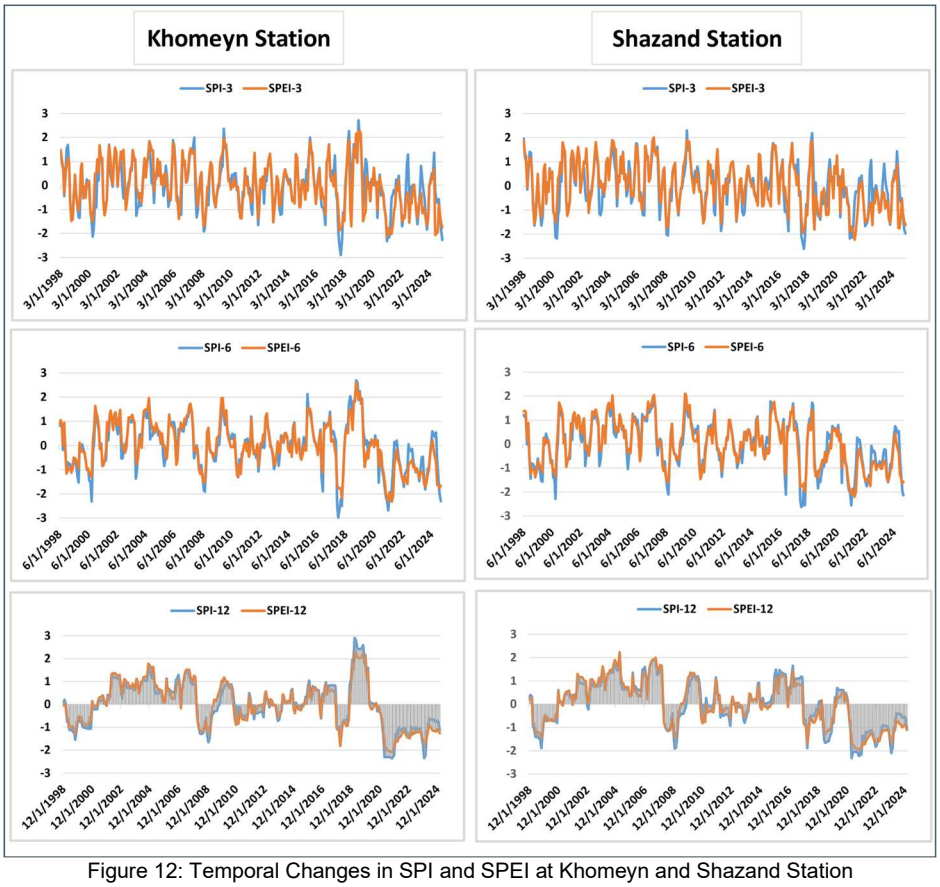

Figure 12: Temporal Changes in SPI and SPEI at Khomeyn and Shazand Station

Journal of Asian Geography, 2025, Volume 4 (Issue 2), 46-62
https://doi.org/10.36777/jag2025.4.2.6

4.4 SPI and SPEI Comparison

To examine the relationship between SPI and SPEI, correlation analysis was conducted at the 3-, 6-, and 12-month timescales for all six validated stations. SPI was derived from GPM precipitation, while SPEI was calculated using GPM precipitation and ERA5-Land temperature. This comparison highlights how closely the two indices align at different temporal resolutions in capturing drought variability.

As illustrated in Figure 13, scatter plots for the Arak station show strong agreement between SPI and SPEI, with correlation values of 0.87 (SPI3 vs. SPEI3), 0.94 (SPI6 vs. SPEI6), and 0.97 (SPI12 vs. SPEI12). The trend of increasing correlation with longer accumulation periods was consistent across all stations. Among the six stations, Komijan, Khomeyn, and Shazand exhibited the highest agreement at the 12-month timescale (R = 0.98), indicating nearly identical long-term drought behavior as captured by both indices.

At the 3-month scale, correlation coefficients ranged from 0.87 to 0.90, reflecting slightly greater variability due to the short-term influence of temperature and evapotranspiration captured by SPEI but not by SPI. Komijan (R = 0.90) showed the strongest short-term match, while Mahallat and Arak had the lowest (R = 0.87), though still indicating a strong relationship. Correlations at the 6-month scale ranged from 0.93 to 0.96, further confirming convergence of the indices as drought duration increases.

Overall, the analysis demonstrates a very high degree of coherence between SPI and SPEI across the Meighan Wetland region, particularly at medium and long timescales. While SPI reflects precipitation anomalies, SPEI's inclusion of evapotranspiration adds valuable climatic sensitivity, yet the two indices remain largely consistent in tracking drought evolution. Their combined use provides a robust foundation for drought assessment in semi-arid climates.

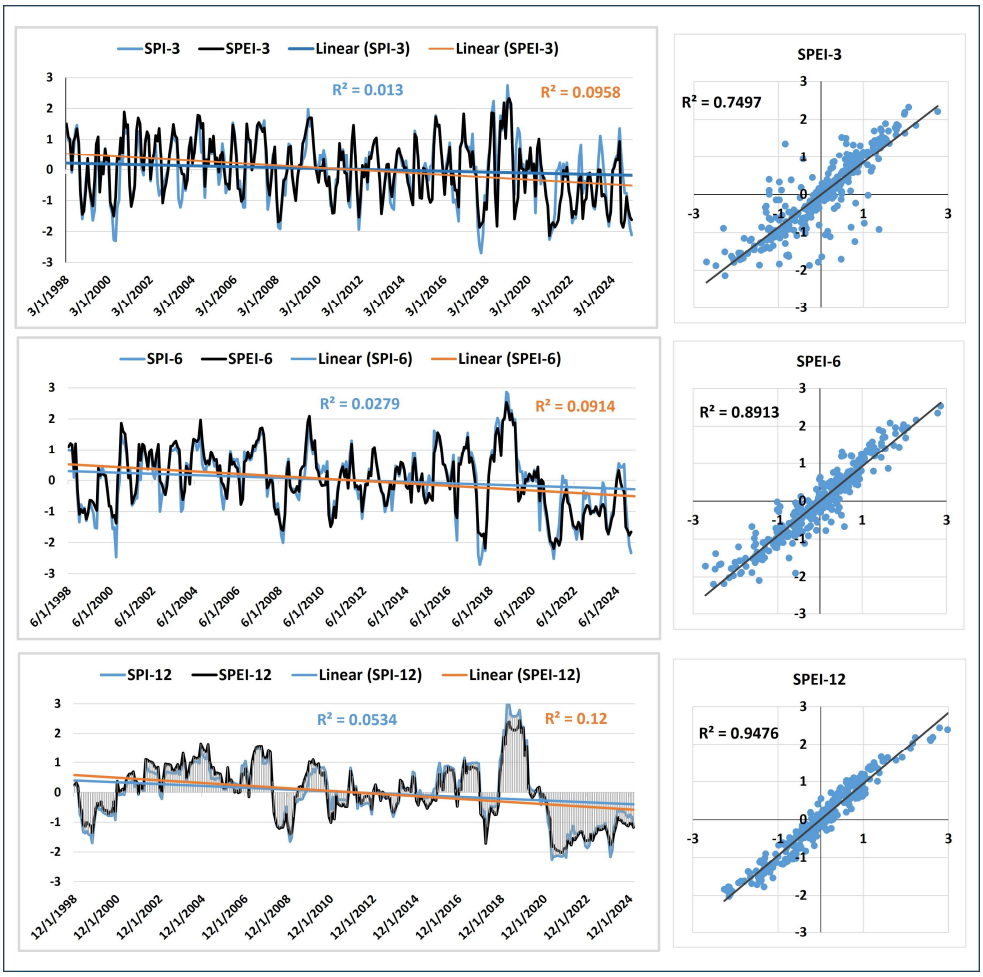

Figure 13: Temporal Changes in SPI and SPEI at Arak Station

4.5 Drought Characteristics

To characterize drought behavior across the Meighan Wetland region, drought event statistics were extracted from SPI records and evaluated in terms of frequency, duration, severity, intensity, and peak SPI values. Figure 14 visualizes the frequency of drought and wet events for all six stations, while Table 5 provides detailed information on specific drought episodes at Arak, Tafresh, and Komijan, the stations most representative of the wetland.

As shown in Figure 14, moderately dry conditions ($-1.5 < SPI \leqslant -1.0$) are the most frequent drought category across all stations, with Arak and Komijan each recording 39 occurrences. Severely dry conditions ($-2.0 < SPI \leqslant -1.5$) were particularly prevalent in Komijan (21 events), suggesting that this station, located in a transitional elevation zone, is more vulnerable to intense rainfall deficits. Although extremely dry events ($SPI \leqslant -2.0$) were less frequent, they occurred across all stations, especially Shazand (11 events) and Mahallat (10 events), indicating localized episodes of extreme hydrological stress. Wet events occurred at similar rates in some stations, but extremely wet conditions ($SPI \geqslant 2.0$) remained rare.

Journal of Asian Geography, 2025, Volume 4 (Issue 2), 46-62
https://doi.org/10.36777/jag2025.4.2.6

Regarding drought structure, Table 5 highlights several prolonged and impactful events. Tafresh experienced the most intense drought, with a minimum SPI of −3.12 during a 6-month event in 2000, accompanied by a severity of −12.18 and an intensity of −2.03. Komijan recorded a drought from April to October 2000 (6 months) with a peak SPI of −2.58 and total severity of −9.88. Although not the longest, this drought had one of the highest intensity values (−1.65), indicating an acute hydrological deficit over a relatively short period. In Arak, the most intense drought also occurred in 2000, lasting 6 months (April to October), reaching a peak SPI of −2.30 and a severity of −9.33. This event was followed by another extreme from October 2017 to April 2018, where SPI dropped to −2.70, with a severity of −10.75, the highest recorded in Arak, and an intensity of −1.79. Notably, this event coincided with widespread regional droughts visible in other indicators, such as SPEI-12, reinforcing its significance in the broader hydroclimatic context of the wetland.

Overall, these findings suggest that while moderate droughts are a recurring seasonal feature, severe and extreme droughts are episodic but highly impactful, often linked to multi-season precipitation anomalies. Tafresh and Komijan tend to experience higher drought intensities, whereas Arak is more prone to broader, prolonged events. This spatial heterogeneity underscores the importance of station-specific monitoring and localized drought preparedness planning across the Meighan watersher.

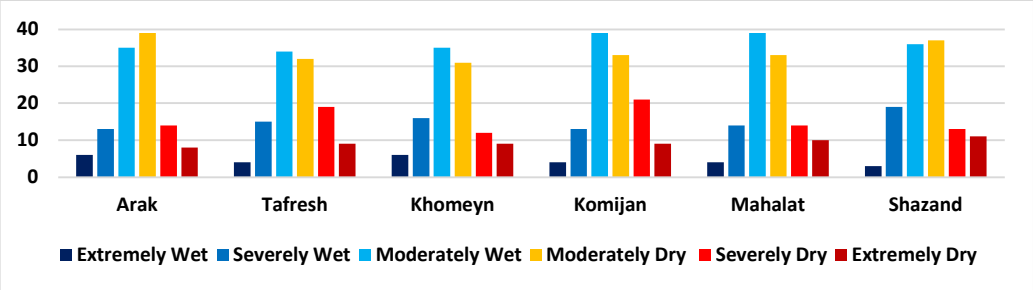

Figure 14: Drought Occurrence Frequency Based on the Intensity of Drought obtained from SPI-3

Table 5: Drought Characteristics

Station Name	Start Date	End Date	Duration	Peak	Severity	Intensity
Arak	Dec 1998	Mar 1999	3	-1.60	-3.11	-1.04
	May 1999	Aug 1999	3	-1.64	-4.02	-1.34
	Apr 2000	Oct 2000	6	-2.30	-9.33	-1.56
	Aug 2003	Jan 2004	5	-1.22	-3.08	-0.62
	Apr 2008	Sept 2008	5	-1.92	-6.04	-1.21
	Oct 2010	Mar 2011	5	-1.28	-4.31	-0.86
	Feb 2012	Apr 2012	2	-1.94	-3.19	-1.60
	Aug 2016	Dec 2016	4	-1.67	-4.89	-1.22
	Oct 2017	Apr 2018	6	-2.7	-10.75	-1.79
	Feb 2021	Aug 2021	6	-2.26	-8.97	-1.50
	Apr 2022	Aug 2022	4	-1.73	-5.87	-1.47
	Dec 2023	Apr 2024	4	-1.83	-4.63	-1.16
Tafresh	Dec 1998	Aug 1999	8	-1.59	-7.59	-0.95
	Apr 2000	Oct 2000	6	-3.12	-12.18	-2.03
	Aug 2003	Jan 2004	5	-1.49	-3.84	-0.77
	Aug 2006	Oct 2006	2	-1.47	-2.75	-1.38
	Apr 2008	Oct 2008	6	-2.05	-6.91	-1.15
	Aug 2010	Mar 2011	7	-1.45	-6.21	-0.89
	Feb 2012	Apr 2012	2	-2.38	-3.68	-1.84
	Aug 2016	Dec 2016	4	-1.60	-5.84	-1.46
	Oct 2017	Feb 2018	6	-2.91	-10.61	-1.77
	Sep 2018	Oct 2018	1	-1.49	-1.49	-1.49
	Feb 2021	Nov 2021	9	-2.31	-8.59	-0.95
	Apr 2022	Aug 2022	4	-1.46	-4.64	-1.16
	Dec 2023	Mar 2024	3	-1.67	-3.57	-1.19
Komijan	Nov 1998	Aug 1999	9	-1.92	-9.69	-1.08
	Apr 2000	Oct 2000	6	-2.58	-9.88	-1.65
	Aug 2003	Oct 2003	2	-1.79	-3.57	-1.79
	Aug 2006	Oct 2006	2	-1.51	-2.89	-1.45
	Apr 2008	Oct 2008	6	-2.18	-6.85	-1.14
	Oct 2010	Mar 2011	5	-1.41	-3.96	-0.79
	Feb 2012	Apr 2012	2	-2.24	-3.40	-1.70
	Aug 2016	Dec 2016	4	-1.60	-5.77	-1.44
	Oct 2017	Feb 2018	4	-2.33	-7.69	-1.92
	Sep 2018	Oct 2018	1	-1.39	-1.39	-1.39
	Feb 2021	Sep 2021	7	-2.16	-9.29	-1.33
	Feb 2022	Sep 2022	7	-1.73	-8.54	-1.22
	Dec 2023	Mar 2024	3	-1.65	-3.80	-1.27

4.6 Monthly Trend Analysis for SPI-3 and SPEI-3 Across Stations

Building on the non-parametric methodology outlined in Section 3.8, monthly trend analyses were applied to SPI-3 and SPEI-3 time series across the six synoptic stations using the MAKESENS v1.0 tool. The Mann–Kendall (MK) test identifies the direction (Z statistic) and significance of monotonic trends, while Sen's slope estimates the rate of change per unit time (Q). The statistical significance levels follow the MAKESENS convention:

- *** Highly significant ($p < 0.001$)
- ** Significant ($p < 0.01$)
- * Moderately significant ($p < 0.05$)
- + Weakly significant ($p < 0.1$)

The SPI-3 trends across all stations were generally weak or non-significant. However, several notable drying patterns emerged (Figure 15):

- Arak displayed a significant drying trend in February (Z = −2.63, Q = −0.072, **) and a weakly significant trend in March (Z = −1.92, Q = −0.045, +).
- Tafresh exhibited a moderately significant decrease in January (Z = −2.42, Q = −0.065, *) and a weak drying signal in February (Z = −1.71, Q = −0.056, +).
- Other stations, including Komijan, Mahallat, Khomeyn, and Shazand, showed no statistically significant SPI3 trends, and Q values were typically near zero, suggesting stable short-term precipitation conditions over time.

These results indicate that, while some localized and seasonal drying trends are emerging—particularly in late winter—the short-term rainfall anomalies represented by SPI-3 remain largely unchanged across the broader region.

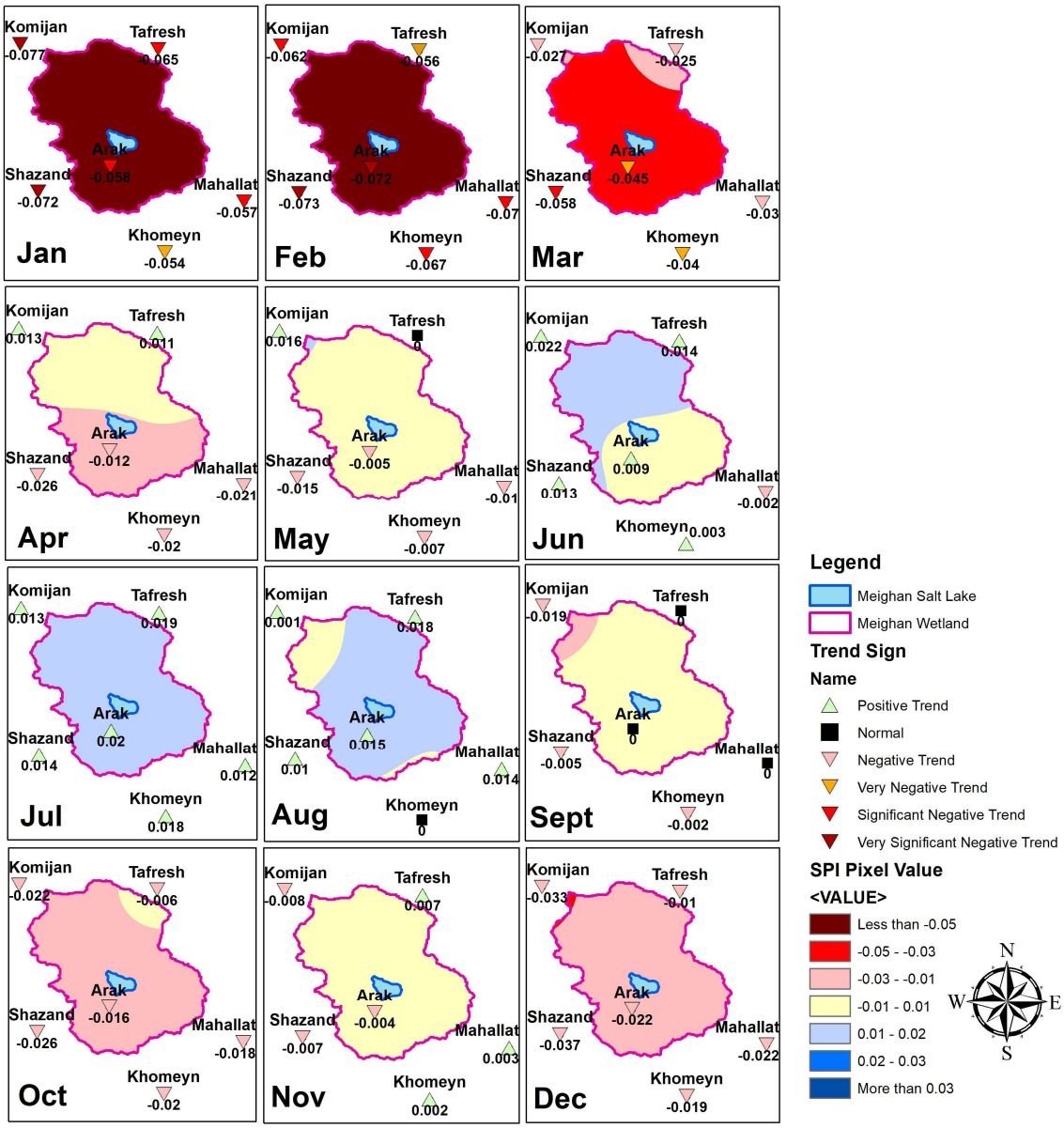

Figure 15: Spatial Distribution of Sen's Slope of SPI3

In contrast to SPI3, the SPEI3 trends showed stronger and more consistent drying patterns, especially in Arak (Figure 16):

- Arak showed statistically significant drying in January (Z = −2.17, Q = −0.063, *), February (Z = −2.71, Q = −0.072, **), March (Z = −2.04, Q = −0.053, *), July (Z = −1.75, Q = −0.045, +), and August (Z = −3.25, Q = −0.087, **).
- These trends suggest that both late winter and late summer in Arak are becoming increasingly drought-prone due to a combination of precipitation deficits and rising evapotranspiration.
- In the other five stations, no statistically significant SPEI3 trends were detected, but some months showed moderate drying tendencies that deserve attention.

While statistical significance was limited to Arak in the SPEI3 analysis, a few other stations showed moderate drying trends without significance, which may indicate emerging or early-stage climatic shifts:

- Khomeyn (January): Q = −0.057, Z = −1.58 (SPEI3)
- Shazand (July): Q = −0.051, Z = −1.50 (SPEI3)

These trends, though not meeting formal significance thresholds, suggest a tendency toward increasing water stress during cooler and warmer seasons, respectively. Overall, the Mann–Kendall and Sen's slope analysis indicates that Arak is the most drought-sensitive station, with significant negative trends in both SPI3 and SPEI3, especially from January to March and in late summer. The lack of significance in other stations suggests spatial variability in drought evolution, possibly influenced by local topography and microclimate. Importantly, the contrast between SPI3 and SPEI3 highlights the growing role of temperature and evapotranspiration in shaping drought patterns, particularly in the transitional months. These findings support the need for multi-index drought monitoring and underscore the value of SPEI in capturing thermal components of water stress under a changing climate.

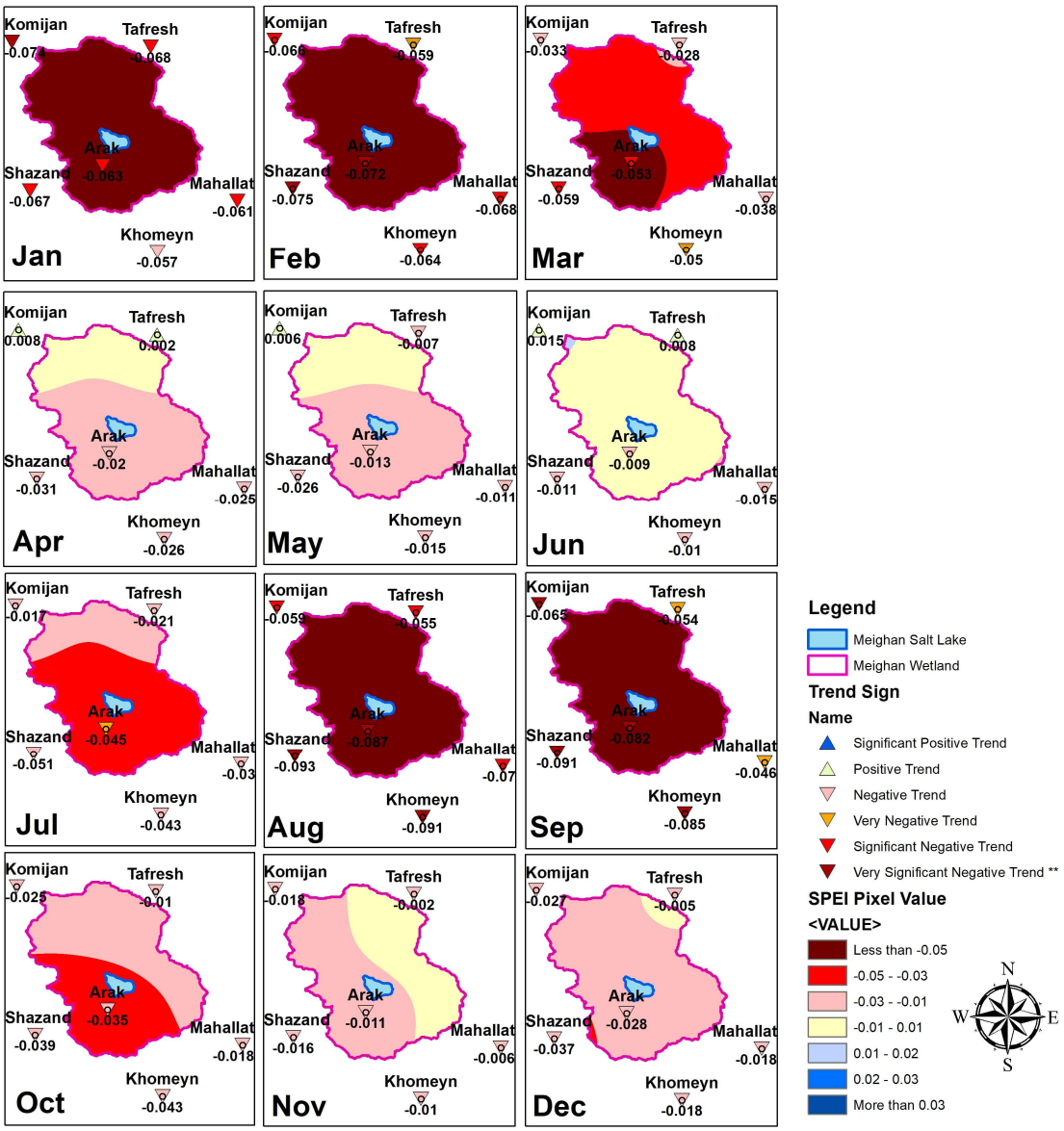

Figure 16: Spatial Distribution of Sen's Slopes of SPEI 3

5.0 Conclusions

This study evaluated the spatiotemporal variability and trends of meteorological drought in the Meighan Wetland region using multi-source precipitation and temperature data. By integrating ground-based synoptic observations with satellite (GPM IMERG) and reanalysis (ERA5-Land) datasets, the research provided a robust assessment of drought patterns through the Standardized Precipitation Index (SPI) and Standardized Precipitation Evapotranspiration Index (SPEI) at 3-, 6-, and 12-month timescales. Validation confirmed the reliability of GPM and ERA5-Land data, showing strong agreement at six stations (Arak, Shazand, Komijan, Mahallat, Khomeyn, and Tafresh; $R > 0.9$ for GPM, $R^2 > 0.98$ for ERA5-Land). Spatial interpolation highlighted elevation-driven rainfall variability, particularly around the Meighan Salt Lake. Major drought episodes in 2000–2001, 2008, 2017–2018, and 2021 were identified, with SPEI indicating greater severity due to rising evapotranspiration. Strong correlations between SPI and SPEI ($R > 0.87$, highest at 12-month scales) supported their combined use. Trend analysis revealed significant drying in Arak during late winter (January–March) and late summer (July–August) via SPEI-3, with moderate drying signals in Khomeyn and Shazand, underscoring the role of temperature in exacerbating drought.

These findings highlight the increasing influence of temperature and atmospheric demand on drought dynamics in semi-arid regions, with implications for wetland sustainability, agricultural water demand, and groundwater recharge in the Meighan basin. To translate these insights into actionable strategies, several policy measures are recommended. First, GPM and ERA5-Land datasets should be adopted for real-time drought monitoring to enhance early warning systems, leveraging their validated accuracy in data-scarce environments. Second, water conservation in Arak should be prioritized, implementing efficient irrigation and groundwater recharge programs to address significant drying trends in late winter and summer. Third, SPEI should be incorporated into regional drought management frameworks to account for evapotranspiration-driven severity, particularly during transitional seasons. Fourth, community preparedness programs, including water conservation training and alternative livelihood strategies, should be developed to mitigate the impacts of severe drought episodes such as those in 2000, 2008, 2017, and 2021. Finally, collaboration among Markazi Province authorities, the Regional Water Company, and the Department of Environment should be fostered to integrate these findings into water allocation and wetland conservation policies. Implementing these measures can strengthen adaptive water resource management and enhance resilience in Iran's vulnerable interior basins.

Future research should extend this analysis by incorporating hydrological and agricultural drought indices, exploring downscaled climate projections, and integrating land-use change scenarios to further inform drought risk assessments and support spatially targeted management strategies.

Acknowledgement: I am also grateful to the School of Humanities, Universiti Sains Malaysia, for providing academic resources and research facilities that enabled this study.

Conflicts of Interest: The author declares that there is no conflict of interest.

References

Ashraf, M., Ullah, K., & Adnan, S. (2022). Satellite based impact assessment of temperature and rainfall variability on drought indices in Southern Pakistan. International Journal of Applied Earth Observation and Geoinformation, 108, 102726. https://doi.org/10.1016/j.jag.2022.102726

Chen, S., Zhang, L., Zhang, Y., Guo, M., & Liu, X. (2020). Evaluation of Tropical Rainfall Measuring Mission (TRMM) satellite precipitation products for drought monitoring over the middle and lower reaches of the Yangtze River Basin, China. Journal of Geographical Sciences, 30(1), 53–67. https://doi.org/10.1007/s11442-020-1723-3

De Jesús, A., Breña-Naranjo, J. A., Pedrozo-Acuña, A., & Alcocer Yamanaka, V. H. (2016). The use of TRMM 3B42 product for drought monitoring in Mexico. Water, 8(8), 325. https://doi.org/10.3390/w8080325

Department of Environment, Iran. (n.d.). Iranian Department of Environment. https://www.doe.ir/portal/home/?140762/%D8%A7%D8%AE%D8%A8%D8%A7%D8%B1%20%D8%A7%D9%86%DA%AF%D9%84%DB%8C%D8%B3%DB%8C

Du, H., Tan, M. L., Chun, K. P., & Zhang, F. (2025). Evaluation of four gridded climate products for streamflow and drought simulations in the Kelantan River Basin, Malaysia. Geocarto International, 40(1), 2453615. https://doi.org/10.1080/10106049.2024.2453615

García-Valdecasas Ojeda, M., Romero-Jiménez, E., Rosa-Cánovas, J. J., Yeste, P., Castro-Díez, Y., Esteban-Parra, M. J., Vicente-Serrano, S. M., & Gámiz-Fortis, S. R. (2021). Assessing future drought conditions over the Iberian Peninsula: The impact of using different periods to compute the SPEI. Atmosphere, 12(8), 980. https://doi.org/10.3390/atmos12080980

Guttman, N. B. (1999). Accepting the standardized precipitation index: A calculation algorithm. Journal of the American Water Resources Association, 35(2), 311–322. https://doi.org/10.1111/j.1752-1688.1999.tb03592.x

Haied, N., Foufou, A., Chaab, S., Azlaoui, M., Khadri, S., Benzahia, K., & Benzahia, I. (2017). Drought assessment and monitoring using meteorological indices in a semi-arid region. Energy Procedia, 119, 518–529. https://doi.org/10.1016/j.egypro.2017.07.072

Irannezhad, M., Marttila, H., Chen, D., & Kløve, B. (2016). Century-long variability and trends in daily precipitation characteristics at three Finnish stations. Advances in Climate Change Research, 7(1–2), 54–69. https://doi.org/10.1016/j.accre.2016.08.002

Jain, V. K., Pandey, R. P., Jain, M. K., & Byun, H.-R. (2015). Comparison of drought indices for appraisal of drought characteristics in the Ken River Basin. Weather and Climate Extremes, 8, 1–11. https://doi.org/10.1016/j.wace.2015.05.001

Kendall, M. G. (1975). Rank correlation methods (4th ed.). Charles Griffin.

Kesarwani, M., Neeti, N., & Chowdary, V. (2023). Evaluation of different gridded precipitation products for drought monitoring: A case study of Central India. Theoretical and Applied Climatology, 151(1), 817–841. https://doi.org/10.1007/s00704-022-04372-5

Khanmohammadi, N., Rezaie, H., & Behmanesh, J. (2022). Investigation of drought trend on the basis of the best obtained drought index. Water Resources Management, 36(4), 1355–1375. https://doi.org/10.1007/s11269-022-03156-9

Liu, C., Yang, C., Yang, Q., & Wang, J. (2021). Spatiotemporal drought analysis by the standardized precipitation index (SPI) and standardized precipitation evapotranspiration index (SPEI) in Sichuan Province, China. Scientific Reports, 11(1), 1280. https://doi.org/10.1038/s41598-020-80993-1

Lotfirad, M., Esmaeili-Gisavandani, H., & Adib, A. (2022). Drought monitoring and prediction using SPI, SPEI, and random forest model in various climates of Iran. Journal of Water and Climate Change, 13(2), 383–406. https://doi.org/10.2166/wcc.2021.210

Mann, H. B. (1945). Nonparametric tests against trend. Econometrica, 13(3), 245–259. https://doi.org/10.2307/1907187

McKee, T. B., Doesken, N. J., & Kleist, J. (1993). The relationship of drought frequency and duration to time scales. In Proceedings of the 8th Conference on Applied Climatology (pp. 179–184). American Meteorological Society.

Mishra, A. K., & Singh, V. P. (2010). A review of drought concepts. Journal of Hydrology, 391(1–2), 202–216. https://doi.org/10.1016/j.jhydrol.2010.07.012

Mishra, A. K., & Singh, V. P. (2011). Drought modeling–A review. Journal of Hydrology, 403(1–2), 157–175. https://doi.org/10.1016/j.jhydrol.2011.03.049

Morid, S., Smakhtin, V., & Moghaddasi, M. (2006). Comparison of seven meteorological indices for drought monitoring in Iran. International Journal of Climatology, 26(7), 971–985. https://doi.org/10.1002/joc.1283

Naumann, G., Barbosa, P., Carrao, H., Singleton, A., & Vogt, J. (2012). Monitoring drought conditions and their uncertainties in Africa using TRMM data. Journal of Applied Meteorology and Climatology, 51(10), 1867–1874. https://doi.org/10.1175/JAMC-D-11-0144.1

Pandey, V., Srivastava, P. K., Singh, S. K., Petropoulos, G. P., & Mall, R. K. (2021). Drought identification and trend analysis using long-term CHIRPS satellite precipitation product in Bundelkhand, India. Sustainability, 13(3), 1042. https://doi.org/10.3390/su13031042

Regional Water Company of Markazi (RWCM). (n.d.). Regional Water Company of Markazi. https://www.marw.ir/?l=EN#

Samantaray, A. K., Ramadas, M., & Panda, R. K. (2022). Changes in drought characteristics based on rainfall pattern drought index and the CMIP6 multi-model ensemble. Agricultural Water Management, 266, 107568. https://doi.org/10.1016/j.agwat.2022.107568

Santos, C. A. G., Brasil Neto, R. M., Passos, J. S. d. A., & da Silva, R. M. (2017). Drought assessment using a TRMM-derived standardized precipitation index for the upper São Francisco River basin, Brazil. Environmental Monitoring and Assessment, 189(6), 250. https://doi.org/10.1007/s10661-017-5968-1

Sen, P. K. (1968). Estimates of the regression coefficient based on Kendall's tau. Journal of the American Statistical Association, 63(324), 1379–1389. https://doi.org/10.1080/01621459.1968.10480934

Spinoni, J., Naumann, G., Vogt, J. V., & Barbosa, P. (2015). The biggest drought events in Europe from 1950 to 2012. Journal of Hydrology: Regional Studies, 3, 509–524. https://doi.org/10.1016/j.ejrh.2015.01.011

Tan, M. L., Tan, K. C., Chua, V. P., & Chan, N. W. (2017). Evaluation of TRMM product for monitoring drought in the Kelantan River Basin, Malaysia. Water, 9(1), 57. https://doi.org/10.3390/w9010057

Tan, M. L., Zhang, F., Juinn, C., Derek, C., Yu, K. H., Shaharudin, S. M., Chan, N. W., & Asyirah, A. R. (2022). Spatio-temporal analysis of precipitation, temperature and drought from 1985 to 2020 in Penang, Malaysia. Water Supply, 22(5), 4757–4768. https://doi.org/10.2166/ws.2021.051

Torres-Vázquez, M. Á., Halifa-Marín, A., Montávez, J. P., & Turco, M. (2023). High resolution monitoring and probabilistic prediction of meteorological drought in a Mediterranean environment. Weather and Climate Extremes, 40, 100558. https://doi.org/10.1016/j.wace.2023.100558

Touma, D., Ashfaq, M., Nayak, M. A., Kao, S.-C., & Diffenbaugh, N. S. (2015). A multi-model and multi-index evaluation of drought characteristics in the 21st century. Journal of Hydrology, 526, 196–207. https://doi.org/10.1016/j.jhydrol.2015.01.007

Tuan, N. H., & Canh, T. T. (2021). Analysis of trends in drought with the non-parametric approach in Vietnam: A case study in Ninh Thuan Province. American Journal of Climate Change, 10(1), 51. https://doi.org/10.4236/ajcc.2021.101004

Ullah, I., Ma, X., Yin, J., Asfaw, T. G., Azam, K., Syed, S., Liu, M., Arshad, M., & Shahzaman, M. (2021). Evaluating the meteorological drought characteristics over Pakistan using in situ observations and reanalysis products. International Journal of Climatology, 41(9), 4437–4459. https://doi.org/10.1002/joc.7144

Vicente-Serrano, S. M., Beguería, S., & López-Moreno, J. I. (2010). A multiscalar drought index sensitive to global warming: The standardized precipitation evapotranspiration index. Journal of Climate, 23(7), 1696–1718. https://doi.org/10.1175/2009JCLI2909.1

Wang, F., Lai, H., Li, Y., Feng, K., Zhang, Z., Tian, Q., Zhu, X., & Yang, H. (2022). Dynamic variation of meteorological drought and its relationships with agricultural drought across China. Agricultural Water Management, 261, 107301. https://doi.org/10.1016/j.agwat.2022.107301

Winkler, K., Gessner, U., & Hochschild, V. (2017). Identifying droughts affecting agriculture in Africa based on remote sensing time series between 2000–2016: Rainfall anomalies and vegetation condition in the context of ENSO. Remote Sensing, 9(8), 831. https://doi.org/10.3390/rs9080831